ACS OMEGA

http://pubs.acs.org/journal/acsodf

Article

Evaluation of 2,3-Dihydro-1,5-benzothiazepine Derivatives as Potential Tyrosinase Inhibitors: *In Vitro* and *In Silico* Studies

Munirah M. Al-Rooqi, Amina Sadiq, Rami J. Obaid, Zaman Ashraf,* Yasir Nazir, Rabab S. Jassas, Nafeesa Naeem, Meshari A. Alsharif, Syed Wadud Ali Shah, Ziad Moussa, Ehsan Ullah Mughal,* Abdel-Rahman Farghaly, and Saleh A. Ahmed*

Cite This: *ACS Omega* 2023, 8, 17195−17208

Read Online

ACCESS | Metrics & More | Article Recommendations | Supporting Information

ABSTRACT: Benzothiazepines are pharmacologically active compounds, frequently utilized as a precursor for acquiring versatile molecules with several bioactivities including anti-inflammatory, anti-human immunodeficiency virus (anti-HIV), analgesic, antitumor, antimicrobial, and antitubercular. In this study, the 2,4-diphenyl-2,3-dihydro-1,5-benzothiazepine scaffold was selected for their *in vitro*, docking, and druglikeness studies to evaluate their inhibitory potential against mushroom tyrosinase. All synthesized analogues, **1**−**14**, exhibited moderate to good IC_{50} values ranging from 1.21 to 70.65 μM. The synthesized benzothiazepine derivatives were potent tyrosinase inhibitors, which outperformed the reference kojic acid (IC_{50} = 16.69 μM). The kinetic analysis revealed that compound **2** (2-(3,4-dimethoxyphenyl)-4-(*p*-tolyl)-2,3-dihydrobenzo[*b*][1,4]thiazepine) was a mixed-type tyrosinase inhibitor with a K_i value of 1.01 μM. Molecular modeling studies against tyrosinase protein (PDB ID: 2Y9X) were conducted to recognize the binding modes of these analogues. The utilization of molecular dynamic (MD) simulations enabled the assessment of the protein−ligand complex's dynamic behavior, stability, and binding affinity for the compounds. These simulations ultimately led to the identification of compound **2** as a potential inhibitor of tyrosinase. Additionally, a druglikeness study was conducted, which supported the promising potential of the new analogues as novel antityrosinase agents. The *in silico* studies were consistent with the *in vitro* results, showing that these ligands had good binding scores against tyrosinase and interacted with the core residues of the target protein. Gaussian 09 was used for the geometry optimization of all complexes.

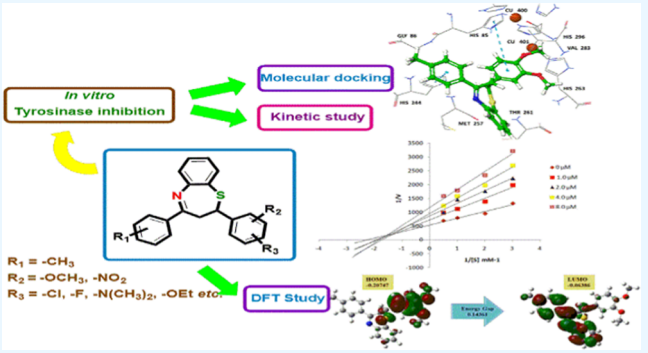

1. INTRODUCTION

Tyrosinase (TYR) (EC 1.14.18.1) is a multifunctional copper-containing oxidase enzyme and broadly disseminated in plants, bacteria, fungi, animals, and mammals.[1] TYR catalyzes melanin biosynthesis in a two-step reaction: *o*-hydroxylation of monophenols to *o*-diphenols (monophenolase) and oxidation of *o*-diphenols to *o*-quinones (diphenolase).[2] These quinones can spontaneously polymerize to form melanin, which determines the color of the mammalian skin and hair. However, excessive epidermal pigmentation can lead to melasma, age spots, and other dermatological disorders.[3−5] Consequently, TYR inhibitors have become more crucial for pharmaceutical and dermatological products that may be used to treat or prevent hyperpigmentation.

TYR is connected to neurodegenerative disorders in patients suffering from Parkinson's disease. TYR is specifically connected to three metabolic processes in insects, including cuticle sclerotization, protective encapsulation, and melanization of invading organisms and wound healing.[5,6] Therefore, TYR's involvement in such crucial activities offers viable targets for creating safer and more efficient TYR inhibitors as pesticides and for controlling them.[7]

Several synthetic heterocyclic TYR inhibitors have been discovered in previous years and found to have antimelanogenic properties.[2,3,8−11] Numerous synthetic heterocyclic TYR inhibitors showed excellent activity against mushroom TYR compared with the standard kojic acid.[11,12] Kojic acid and hydroquinone have been reported to be dangerous for human skin at the intensities essential for their depigmenting actions.[13]

Benzothiazepine (Figure 1) is a desirable motif in pharmaceutical chemistry and is regarded as a thiazepine derivative.[14,15] This pharmacophore plays a vital role in drug discovery programs due to its derivatives exhibiting a wide range

Received: March 8, 2023
Accepted: April 20, 2023
Published: May 4, 2023

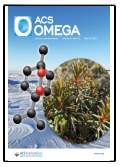

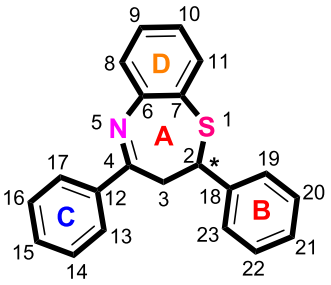

Figure 1. Chemical structure of 2,3-dihydro-1,5-benzothiazepine.

of biological activities such as central nervous system (CNS) depressant, calcium antagonism, antifeedant, antimicrobial, anti-human immunodeficiency virus (anti-HIV), anticonvulsant, bradykinin receptor antagonist, and calmodulin antagonist.[16] Numerous bioactive heterocycles exhibiting TYR inhibitory potential have been reported in the literature. The existence of electronegative N-, O-, and S-atoms in the potent inhibitor structure enhances the coordination capacities of compounds.[17]

Currently, benzothiazepines are among the very broadly used pills in the treatment of cardiovascular diseases, including examples such as thiazesim, clentiazem, and diltiazem[18] (Figure 2). Benzothiazepine analogues have shown activity against various target proteins and are of particular interest for lead development.[19]

Inspired by the therapeutic importance of the benzothiazepine scaffold[14] and in the perpetuation of our concern in creating new antityrosinase compounds,[8,10,14,20] herein, we report benzothiazepine as a potential TYR inhibitor. The novelty of this study lies in the investigation of the benzothiazepine scaffold for its potential tyrosinase inhibitory activity, which has not been previously explored. To the best of our knowledge, this heterocyclic core has not been investigated earlier, and we for the first time report this motif against TYR. Thus, the potential of benzothiazepine derivatives as potent TYR inhibitors represents a promising avenue for the development of new treatments for hyperpigmentation disorders, such as melasma and age spots. All the target analogues were accessed for their *in vitro* TYR inhibitory activity. *In silico* investigations were carried out on these analogues to better explore their interactions with the active site of TYR.

2. RESULTS AND DISCUSSION

2.1. Chemistry. The subject compounds **1**−**14** were prepared by Michael's addition of 2-aminothiophenol to chalcones in the presence of hexafloroisopropanol (HFIP) solvent at ambient temperature to furnish the target compounds **1**−**14** in moderate to good yields (Scheme 1). The complete synthesis and spectroscopic data of the target analogues are already given in the literature[14] and also in the Supporting Information (SI) file.

2.2. Mushroom TYR Inhibitory Study. Continuing our previous analysis of mushroom TYR inhibition, benzothiazepines **1**−**14** were assessed for their activity against the enzyme. All of the targeted analogues, **1**−**14**, showed moderate to good inhibitory activity against the TYR enzyme (Table 1).

Table 1 demonstrates the IC_{50} of the target analogues and standard kojic acid (IC_{50} = 16.69 μM). The analogues **1**−**14** exhibited IC_{50} values in the range of 1.21−70.65 μM. Among the target benzothiazepines, analogue **2** revealed excellent TYR inhibition with the lowest IC_{50} = 1.21 μM. Moreover, analogues **3** (IC_{50} = 10.42 μM), **4** (IC_{50} = 13.24 μM), **6** (IC_{50} = 12.27 μM), and **13** (IC_{50} = 1.34 μM) exhibited outstanding TYR inhibitory activity as compared to the reference standard. Furthermore, the analogues **1** (IC_{50} = 38.69 μM), **5** (IC_{50} = 20.12 μM), **7** (IC_{50} = 30.51 μM), **8** (IC_{50} = 22.41 μM), **9** (IC_{50} = 30.74 μM), **10** (IC_{50} = 50.89 μM), **11** (IC_{50} = 70.65 μM), **12** (IC_{50} = 39.58 μM), and **14** (IC_{50} = 52.68 μM) displayed moderate to good inhibitory activity and could be suggested as promising candidates for TYR-mediated hyperpigmentation.

2.3. Kinetic Studies. To identify the inhibition type of compound **2** on the diphenolase activity of the L-3,4-

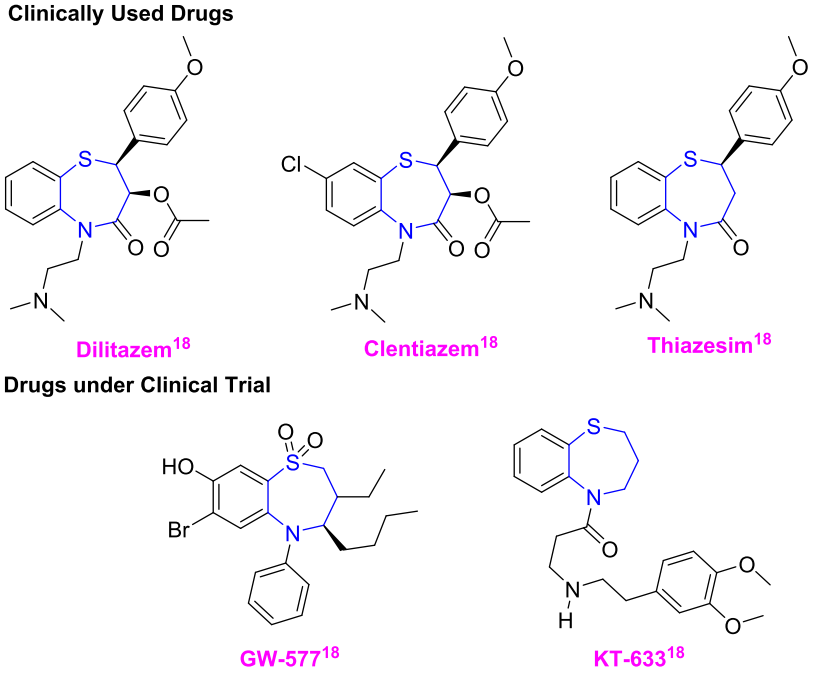

Figure 2. Representative benzothiazepine derivatives either in clinical use or currently undergoing clinical trials.

https://doi.org/10.1021/acsomega.3c01566
ACS Omega 2023, 8, 17195−17208

Scheme 1. Synthesis of 1,5-Benzothiazepines 1−14

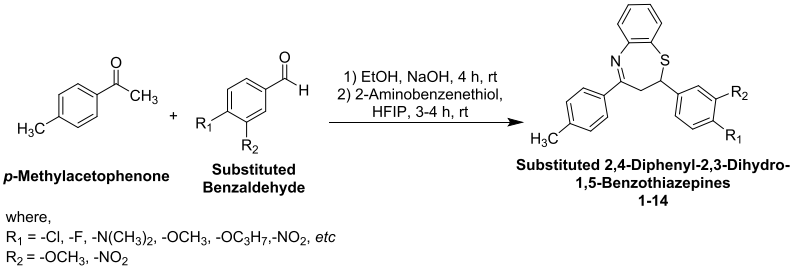

Compound No.	Chemical Structures	Compound No.	Chemical Structures
1	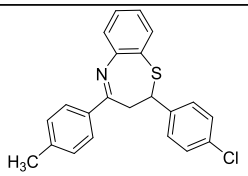	8	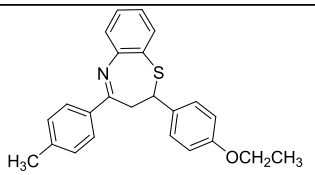
2	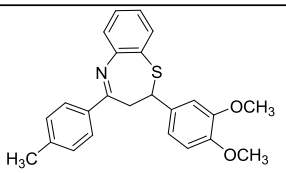	9	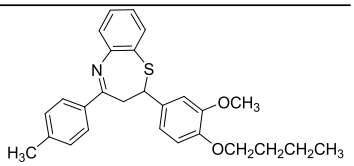
3	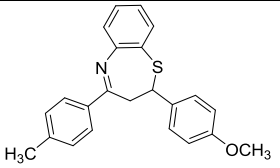	10	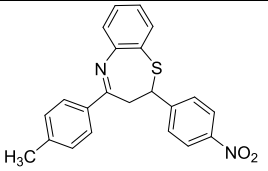
4	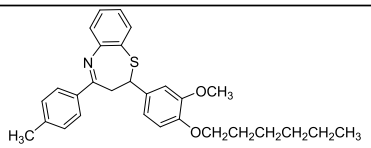	11	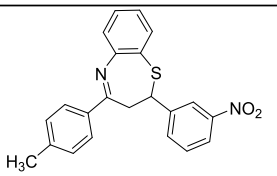
5	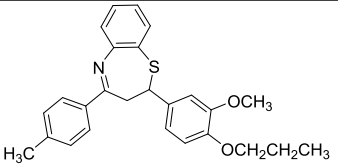	12	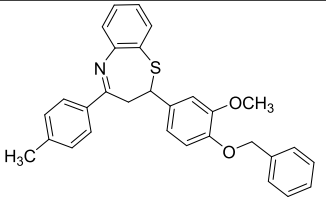
6	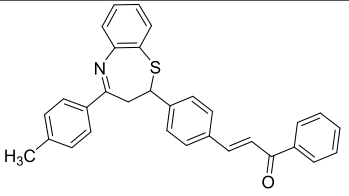	13	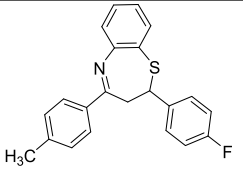
7	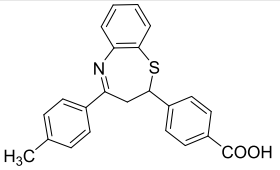	14	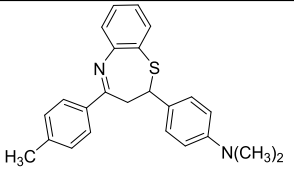

dihydroxyphenylalanine (L-DOPA) oxidation, Lineweaver−Burk plots were employed. The enzyme kinetics in the presence of compound **2** are presented in Figure 3A,B. The family of straight lines with different slopes was obtained by plotting $1/V$ *versus* $1/[S]$. The study demonstrated that compound **2** operates through two separate pathways to inhibit TYR and shows mixed-

https://doi.org/10.1021/acsomega.3c01566
ACS Omega 2023, 8, 17195−17208

Table 1. TYR Inhibitory Efficacy of Benzothiazepines 1−14

compound no.	% inhibition at 25 μg/mL	mushroom TYR inhibition $IC_{50} \pm SEM^a$ (μM)	compound no.	% inhibition at 25 μg/mL	mushroom TYR inhibition $IC_{50} \pm SEM^a$ (μM)
1	34 ± 1	38.69 ± 2.35	**8**	45 ± 2	22.41 ± 1.82
2	89 ± 3	1.21 ± 0.05	**9**	63 ± 3	30.74 ± 3.23
3	23 ± 1	10.42 ± 1.01	**10**	21 ± 1	50.89 ± 4.19
4	19 ± 2	13.24 ± 2.56	**11**	13 ± 2	70.65 ± 4.98
5	38 ± 1	20.12 ± 3.08	**12**	28 ± 1	39.58 ± 2.88
6	54 ± 3	12.27 ± 1.71	**13**	76 ± 3	1.34 ± 2.98
7	32 ± 2	30.51 ± 4.52	**14**	25 ± 1	52.68 ± 3.12
kojic acid (standard)	100	16.69 ± 0.81			

[a]IC_{50} values (mean ± standard error of the mean).

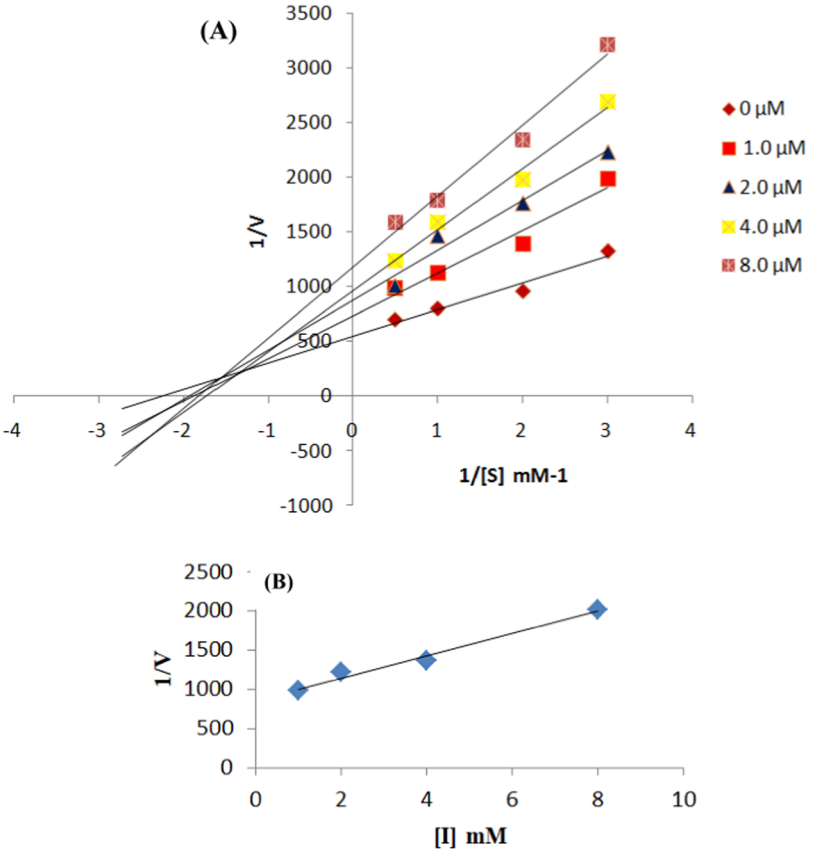

Figure 3. (A) Determination of the inhibition type of compound **2** by a Lineweaver−Burk plot, the inhibitor **2** with concentrations (0.0, 1.0, 2.0, 4.0, and 8.0 μM). (B) Secondary plot between $1/V_{max}$ and various concentrations of compound **2**.

type inhibition, as evidenced by the decrease in V_{max} and the alteration of K_m with increasing concentrations of compound **2**. The V_{max} decreased with changing K_m by increasing concentrations of compound **2** showed mixed-type inhibition having a K_i value of 1.01 μM.

2.4. Structure−Activity Relationship (SAR). It is possible to conduct a simple SAR analysis of the examined compounds because the results of the IC_{50} determination and docking score are consistent and remain in agreement. On the phenyl ring B of the 2,4-diphenyl-2,3-dihydro-1,5-benzothiazepine motif, the type and position of substituents appear to have a significant impact on the compound's activity (Figure 4).

Introducing a methoxy (−OCH_3) group at the meta and para positions of ring B (compound **2** IC_{50} = 1.21 μM and docking score = −7.58 kcal/mol) and *p*-CH_3 substitution on ring C increased inhibitory activity by 14-fold more than the standard (kojic acid IC_{50} = 16.69 μM and docking score = −4.291 kcal/mol).

The strongest inhibitor among those shown was produced by adding another chalcone moiety, which significantly boosted the inhibitory constant and docking score. Due to the fact that such a substitution leads to a bulky molecule, it produced the third-best compound among all the entities examined (compound **6** IC_{50} = 12.27 μM and docking score = −6.75 kcal/mol).

In the case of the most intense inhibitor (compound **3** IC_{50} = 10.42 μM and docking score = −7.40 kcal/mol), the −OCH_3 group present at the para position enhanced the inhibitory potency due to a better interface with the enzyme active pockets.

Furthermore, compound **4** (IC_{50} = 13.24 μM and docking score = −6.78 kcal/mol) having *p*-OC_6H_{13} and *m*-OCH_3 substitution on ring B and *p*-CH_3 substitution on ring C showed better inhibitory activity as compared to the standard kojic acid

https://doi.org/10.1021/acsomega.3c01566
ACS Omega 2023, 8, 17195−17208

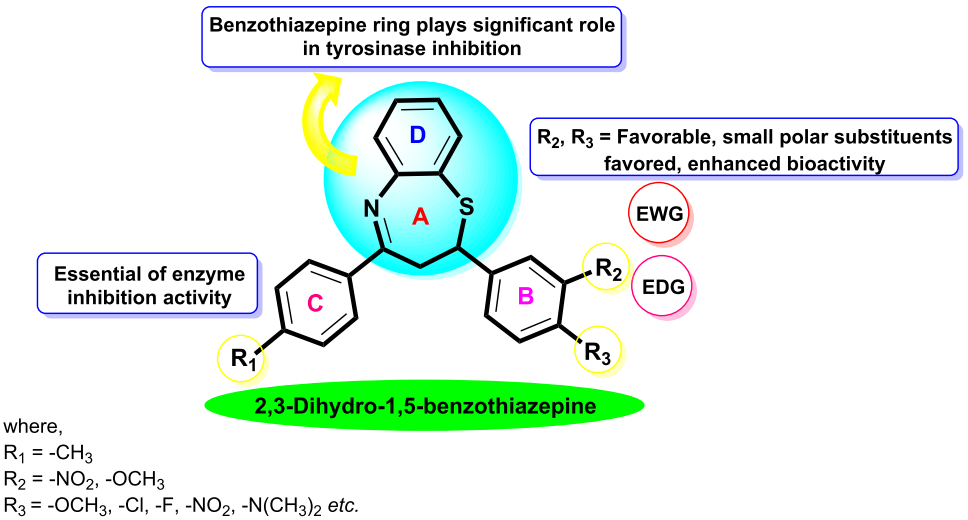

Figure 4. SAR of the studied compounds **1**−**14**.

(IC_{50} = 16.69 μM and docking score = −4.291 kcal/mol). The electronegativity of one *m*-OCH_3 group and one *p*-OC_4H_9 group of the phenyl ring (ring B), which appropriately interact with the enzyme active site, may be the cause of the significant inhibitory potential.

Additionally, compound **13** (IC_{50} = 1.34 μM and docking score = −7.12 kcal/mol) bears *p*-F on ring B. This substitution appears to be situated on the ring in a way that will promote a good fitting with the enzyme's active pocket. All compounds **1**−**14** embrace different electron-donating and -withdrawing substitutions on ring B, which could potentially enhance or lower the inhibitory activity of target analogues.

2.5. Molecular Docking Studies. The crystal structure of mushroom TYR (PDB ID 2Y9X) was used to dock the synthesized compounds **1**−**14** using the Glide dock XP module. The resulting binding energies ranged from −5.28 to −7.58 kcal/mol, indicating moderate to good interactions (Table 2).

Table 2. Binding Energies (kcal/mol) of TYR (2Y9X) with Target Compounds 1−14

compound no.	docking score (kcal/mol)	compound no.	docking score (kcal/mol)
1	−5.86	**8**	−6.69
2	−7.58	**9**	−6.18
3	−7.40	**10**	−6.45
4	−6.72	**11**	−5.31
5	−6.47	**12**	−5.75
6	−6.75	**13**	−7.12
7	−6.31	**14**	−5.28
kojic acid (standard)	−4.291 kcal/mol		

Key amino acid residues involved in binding included arginine, alanine, glycine, valine, proline, methionine, phenylalanine, histidine, and conserved copper (Cu^{2+}) ions. The docking images of the docked complexes (Figures 5a,b, 6a,b, 7a,b and 8a,b) confirmed the previously reported findings.[21,22] Compounds **2**, **3**, **6**, and **13** demonstrated good inhibition, indicating effective blocking of active site amino acids by occupying the inside surface grooves. However, the rigid structures of these molecules prevent them from penetrating into the active site, predicting their mixed-type inhibition.

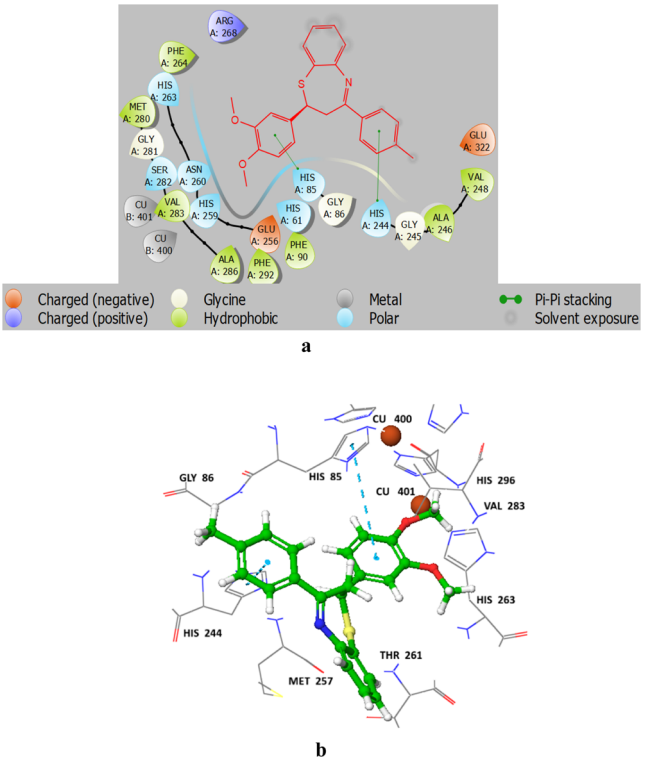

Figure 5. (a) Ball and stick docking 2D image of compound **2**. (b) Ball and stick docking 3D image of compound **2**.

Compound **2** displayed the best docking score (−7.58 kcal/mol), and its toluene moiety's phenyl ring is predicted to strongly interact with the active site residue His244 through $\pi-\pi$ stacking. Additionally, the dimethoxy-substituted phenyl ring of this compound is involved in another $\pi-\pi$ interaction with His85, further stabilizing the protein inhibitor complex (Figure 5a,b). The thiazepine moiety's bulky size prevents this compound from entering the active site, thus predicting its mixed-type inhibition.

The methoxy-substituted aryl ring of the second-best docking score (−7.40 kcal/mol) compound **3** interacts through π interactions with amino acid His244, and the remaining part of the ligand is further stabilized by another π−cationic interaction

https://doi.org/10.1021/acsomega.3c01566
ACS Omega 2023, 8, 17195−17208

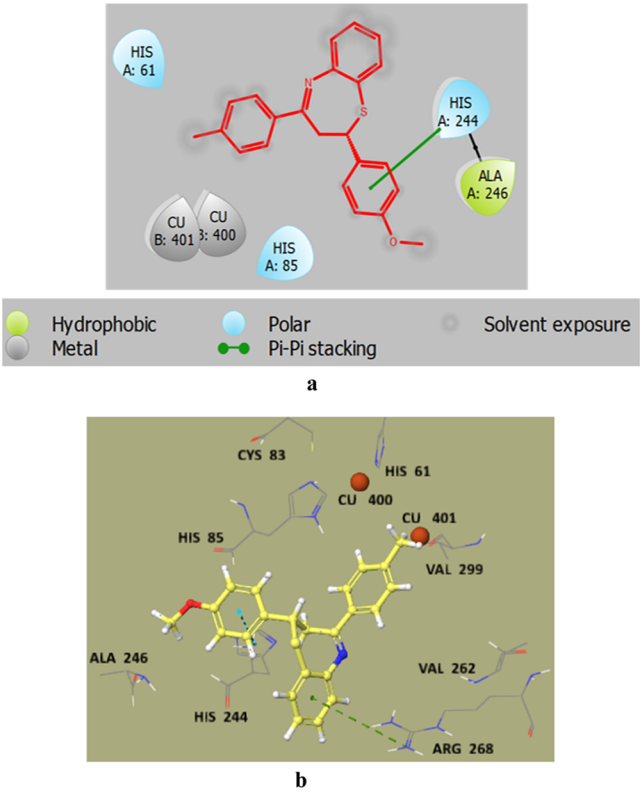

Figure 6. (a) Ball and stick docking 2D image of compound **3**. (b) Ball and stick docking 3D image of compound **3**.

with the active site residue Arg268. The rigid structure of **3** prevents it from entering the enzymatic pocket and lies at the opening of the active site (Figure 6a,b).

The third most potent and active compound both in enzymatic (IC_{50} = 19.27 μM) and computational studies (−6.75 kcal/mol) was **6**. The α,β unsaturated carbonyl moiety forms a strong H-bond interaction with the active site-conserved residue His85 (2.55 Å), and this phenyl ring is further stabilized by $\pi-\pi$ stacking with neighboring residues His263 and Phe264 (Figure 7a,b).

The next active compound both in enzymatic (IC_{50} = 1.34 μM) and computational studies (−7.12 kcal/mol) was **13**. The benzothiazepine moiety is predicted to form $\pi-\pi$ stacking with neighboring residues Arg268 and Phe264 (Figure 8a,b).

2.6. Molecular Dynamic (MD) Simulations. The root mean square deviation (RMSD) of protein backbone atoms was measured to explore the stability of complex **2** (Figure 9A). RMSD analysis revealed that the backbone atoms deviated to ∼2 Å at 20 ns, and then, it gradually decreased to ∼1.5 Å at 30. After attaining this confirmation, the atoms did not show deviations and remained stable till 100 ns, indicating the stability of the complex. Similarly, the radius of gyrations (R_g) was calculated over the simulation time to analyze the compactness of the protein structure. The higher R_g values show the unfolding events in protein during simulation. Figure 9B shows the R_g behavior during simulation. The plot showed that the R_g value was stable throughout the simulation, starting from ∼20.4 Å and remaining in the range of ∼20.5−20.7 Å throughout the simulation, which indicates that the protein structure remained stable during the simulation. To analyze the flexibility of protein residues, root mean square fluctuation was measured and plotted (Figure 9C). The higher RMSF value indicates the

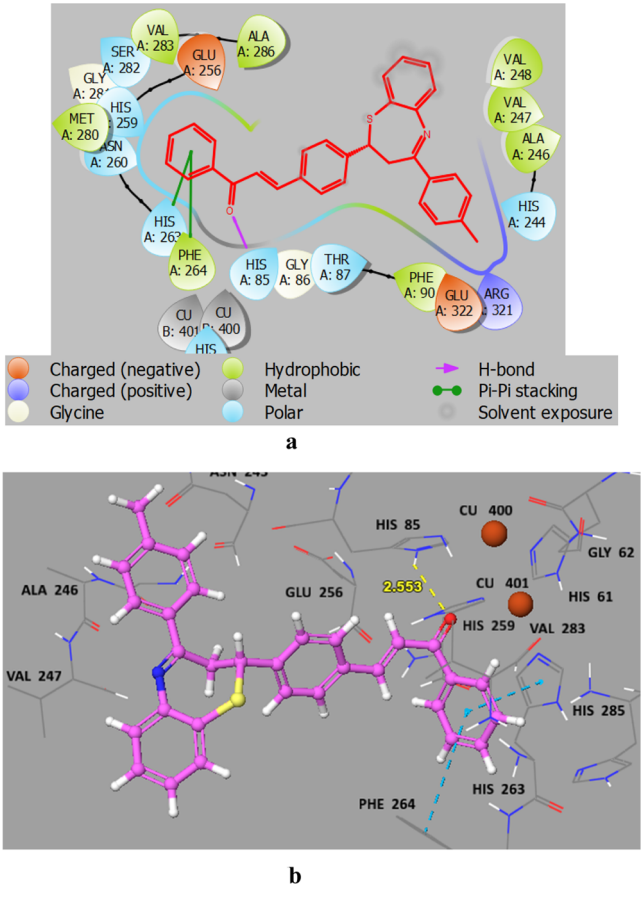

Figure 7. (a) Ball and stick docking 2D image of compound **6**. (b) Ball and stick docking 3D image of compound **6**.

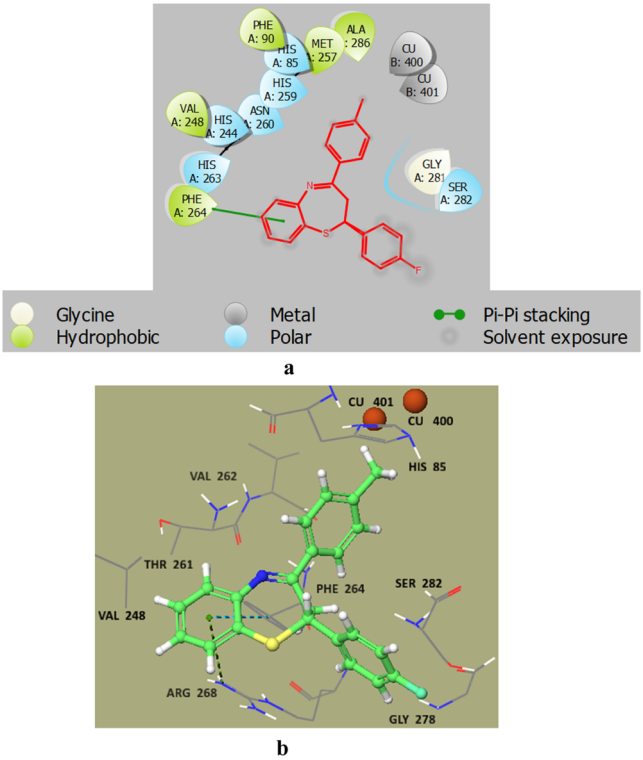

Figure 8. (a) Ball and stick docking 2D image of compound **13**. (b) Ball and stick docking 3D image of compound **13**.

https://doi.org/10.1021/acsomega.3c01566
ACS Omega 2023, 8, 17195−17208

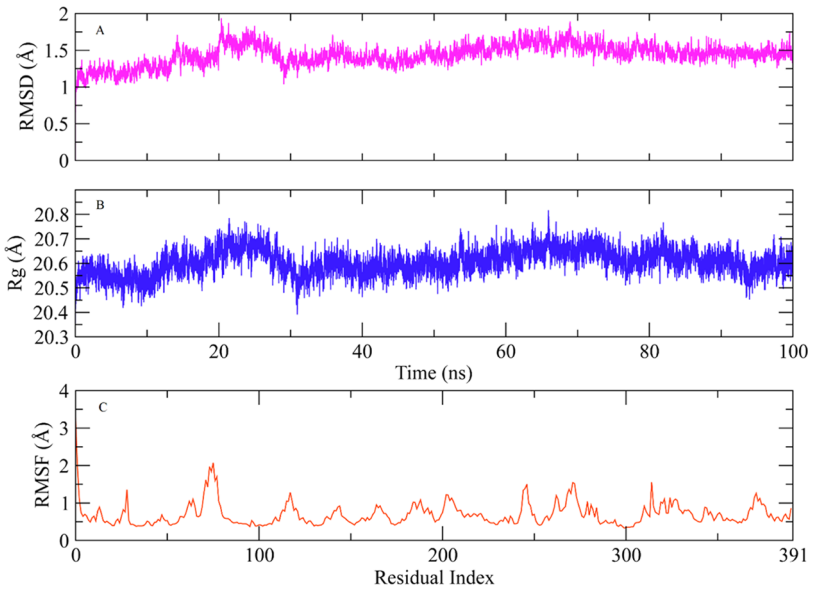

Figure 9. MD trajectory analysis to measure the RMSD, R_g, and RMSF of compound **2**. (A) Root mean square deviation of protein backbone atoms. (B) R_g analysis to measure the compactness of the protein. (C) Flexibility of protein residues with the bound ligand.

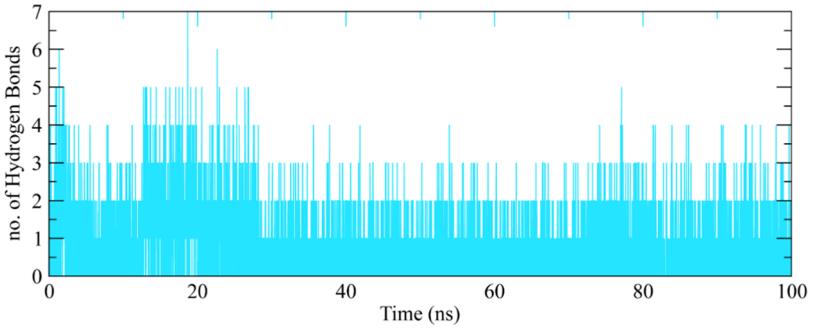

Figure 10. Number of hydrogen bonds formed between the protein and ligand during simulation.

Table 3. HOMO and LUMO Energy Values and Other Related Parameters of 2, 3, 4, 6, 13, and Kojic Acid

parameters (eV)	2	3	4	6	13	kojic acid
E_{LUMO}	−0.06386	−0.06388	−0.06439	−0.08270	−0.07413	−0.05454
E_{HOMO}	−0.20747	−0.21766	−0.21674	−0.22368	−0.21916	−0.23177
energy gap $\lvert E_{HOMO} - E_{LUMO}\rvert$	0.14361	0.15378	0.15235	0.14098	−0.14503	0.17723
ionization potential ($I = -E_{HOMO}$)	0.20747	0.21766	0.21674	0.22368	0.21916	0.23177
electron affinity ($A = -E_{LUMO}$)	0.06386	0.06388	0.06439	0.08270	0.07413	0.05454
chemical hardness ($\eta = (I - A)/2$)	0.071805	0.07689	0.076175	0.07049	0.072515	0.17723
chemical softness ($\zeta = 1/2\eta$)	6.9633	6.5027	6.5638	7.0932	1.511135	2.8211
electronegativity ($\chi = (I + A)/2$)	0.13566	0.14077	0.140565	0.15319	0.146645	0.143155
chemical potential ($\mu = -(I + A)/2$)	−0.13566	−0.14077	−0.140565	−0.15319	−0.146645	−0.143155
electrophilicity index ($\omega = \mu^2/2\eta$)	0.12815	0.12886	0.15235	0.12969	0.148277	0.057815

flexible residues, while the lower value indicates rigid residues. In the RMSF plot, the residues ranging from 170 to 80 showed major fluctuations due to the presence of loops, while the other residues did not show any major fluctuations during the simulation, which indicates that the protein remained rigid and did not show flexibility.

Moreover, the hydrogen bonding in the protein and ligand was analyzed to find complex stability. The hydrogen bonds formed and distorted during the simulation and a higher number of hydrogen bonds show the stability of complex **2**. Figure 10 shows the number of hydrogen bonds formed between the protein and ligand during the simulation. The number of hydrogen bonds went up to 6 at the start of the simulation and then gradually decreased to 3 toward the end of the simulation. The average number of hydrogen bonds during the simulation was 2.5, which indicates the strong binding and stability of the protein−ligand complex.

2.7. Density Functional Theory (DFT). While describing charge creation, the highest occupied molecular orbital (HOMO) (donor) and lowest unoccupied molecular orbital (LUMO) (acceptor) characteristics are very crucial. Since many chemical processes involve electrons directly, the HOMO and LUMO have an impact on how the molecule behaves chemically. Here, the HOMO and LUMO analysis of the

https://doi.org/10.1021/acsomega.3c01566
ACS Omega 2023, 8, 17195−17208

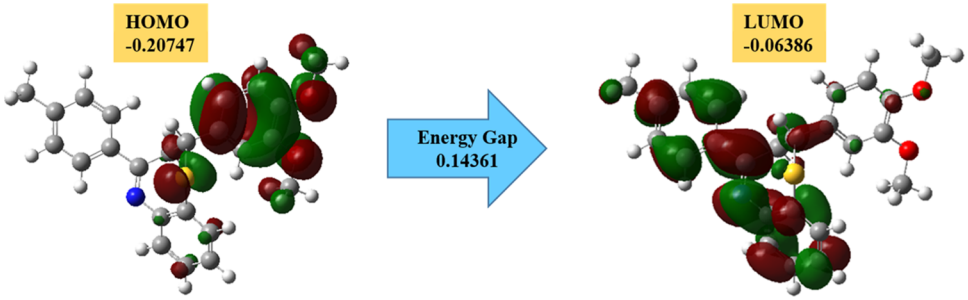

Figure 11. HOMO−LUMO plots of compound **2**.

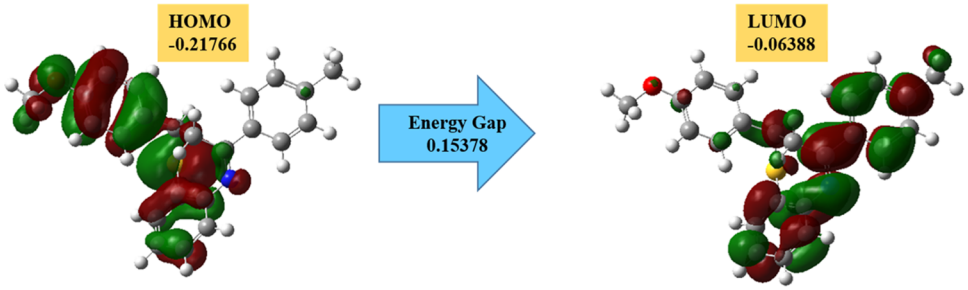

Figure 12. HOMO−LUMO plots of compound **3**.

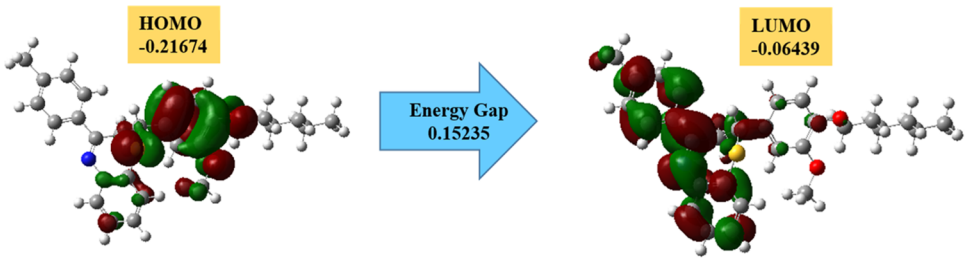

Figure 13. HOMO−LUMO plots of compound **4**.

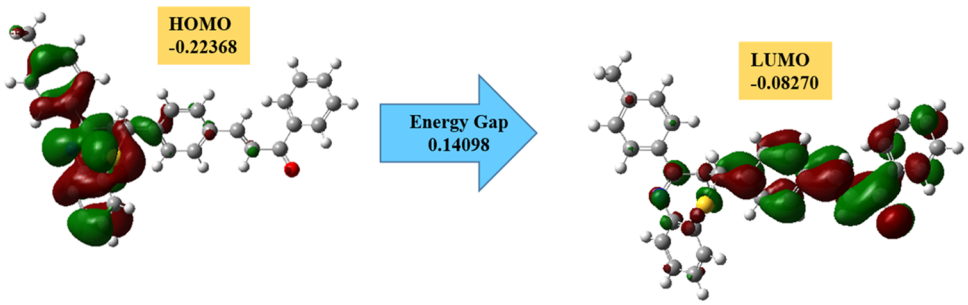

Figure 14. HOMO−LUMO plots of compound **6**.

selected benzothiazepine derivatives **2**, **3**, **4**, **6**, and **13** was accomplished. The HOMO−LUMO energies are well-known quantum mechanical aspects that affect a wide variety of chemical interactions. One of the better findings for explaining the chemical stability of molecules is frontier molecular orbital (FMO) theory, which involves the HOMO and LUMO. HOMO and LUMO energies illustrate information about energy distribution. The stability of compounds is determined by the negative magnitude of E_{HOMO} and E_{LUMO}. The energy gap ($E_{HOMO}-E_{LUMO}$) describes the chemical reactivity and kinetic stability of any molecule. The relative stability of a molecule is determined by its energy gap, with larger gaps indicating greater stability. In this study, the energy gaps for the selected compounds were found to be in the following order: **3** > **4** > **2** > **6** > **13**. These results suggest that compound **3**, which has the highest energy gap, is the most stable among the tested compounds. To calculate these values, quantum calculations were performed using the Gaussian 09 program with the GaussView 5.0.16 interface. The resulting HOMO/LUMO, ionization potential, electron affinity values, and other descriptors were also calculated and are presented in Table 3.

A molecule with a high HOMO−LUMO gap is one that is rigid, tiny, and polarizable. Soft systems are big and highly polarizable, despite having a modest HOMO−LUMO gap. A large HOMO−LUMO gap is associated with strong molecular stability and low reactivity in chemical processes, whereas a small

https://doi.org/10.1021/acsomega.3c01566
ACS Omega 2023, 8, 17195−17208

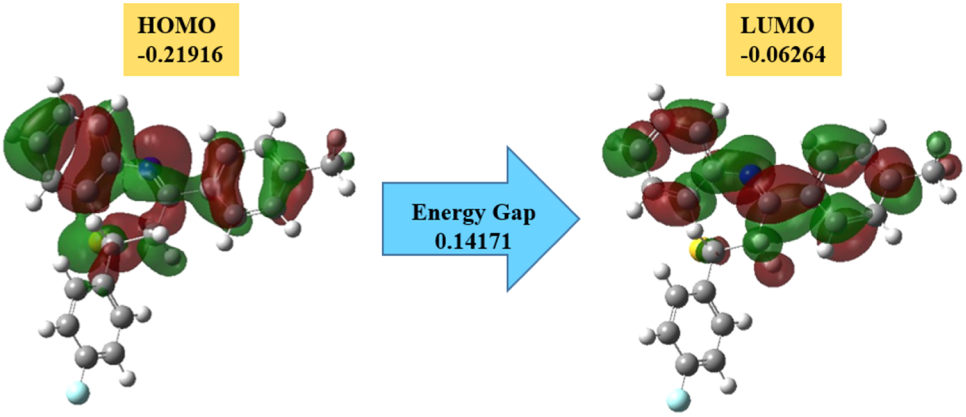

Figure 15. HOMO−LUMO plots of compound **13**.

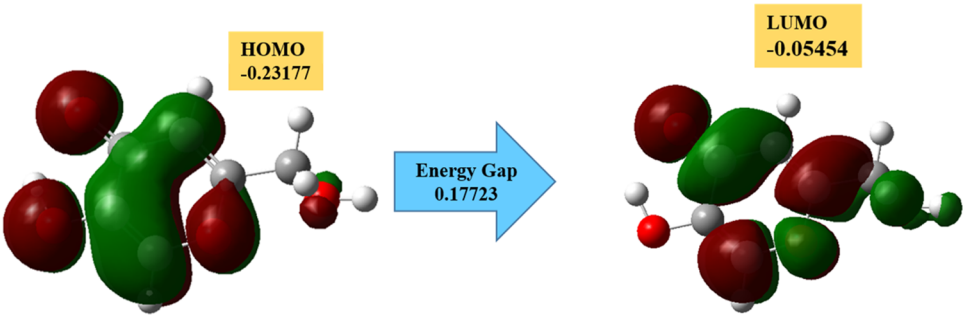

Figure 16. HOMO−LUMO plots of kojic acid (standard).

HOMO−LUMO gap is associated with antiaromaticity. The HOMO and LUMO structures of **2**, **3**, **4**, **6**, **13**, and kojic acid are shown in Figures 11−16. The characteristics of the lowest unoccupied molecular orbital (LUMO) (acceptor) and the highest occupied molecular orbital (HOMO) (donor) are significant for defining the creation of charges. Calculations were made to determine the HOMO/LUMO, ionization potential, energy gap, electron affinity, and other characteristics as a consequence. The energy gap and a molecule with antiaromaticity are used to assess a structure's stability.

2.8. Molecular Electrostatic Potential (MEP). An instrument for anticipating the sites of nucleophilic and electrophilic assault on a molecule is the molecular electrostatic potential (MEP). All of these drugs interact as inhibitors, and the MEP may be an essential tool for validating this. MEP uses color grading to define a molecule's shape, size, and negative, positive, and neutral regions. In the descending order of potential, the colors are red, orange, yellow, green, and blue.

Following the color order makes it very simple to locate places that are advantageous for nucleophile and electrophilic attacks. The color red on the map indicates regions of low electrostatic potential, which imply an excess of electrons and make them a preferred site for an electrophilic attack. Conversely, the color blue shows areas with the highest electrostatic potential, indicating a lack of electrons in that region. DFT calculations with the optimized structure and basis set were used to determine the MEP of the compounds in surface analysis. The electrophilic and nucleophilic components of each chemical are represented by the colors red and green, respectively. The presence of electron-donating and -withdrawing substituents at various positions significantly influenced inhibitory activity.[23]

The mapped electrostatic potential surfaces of the selected compounds are shown in Figure 17.

2.9. Druglikeness Study. Lipinski's rule was used to analyze the target compounds', **1**−**14**, drug-like characteristics to validate their therapeutic applicability (Table 4). The molecular weights of all the synthesized compounds fall within the acceptable range of 500 g/mol or less g/mol. Additionally, Lipinski's rule of 5 is satisfied by H-bond acceptors and donors, which means that they fall within the permissible range. Compounds **1**−**9** and **12**−**14** had a molLog *P* value greater than 5, which implies lower membrane permeability and insufficient solubility. However, compounds **10** and **11** had molLog *P* values below 5, indicating higher permeability and lipid solubility. The findings suggest that some of the analogues were compliant with RO5 and possessed strong drug-like properties, making them potential candidates for drug development.

3. CONCLUSIONS

In summary, a series of synthetic benzothiazepine derivatives were studied for their ability to inhibit TYR activity. All of the target compounds showed a moderate to good inhibition range, with IC_{50} values ranging from 1.21 to 70.65 μM, compared to the standard kojic acid (IC_{50} = 16.69 μM). In the series, compounds **2** (IC_{50} = 1.21 μM), **3** (IC_{50} = 10.42 μM), **4** (IC_{50} = 13.24 μM), **6** (IC_{50} = 12.27 μM), and **13** (IC_{50} = 1.34 μM) showed lower IC_{50} values as compared to the standard and exhibited excellent TYR inhibitory activity. Compound **2** displayed mixed-type behavior based on kinetic analysis. Structure−activity relationship analysis indicated that the presence and position of electron-donating and -withdrawing substituents significantly influenced inhibitory activity. In addition to *in vitro* analysis, which confirmed potent interactions with the target protein and stable complexes with TYR, *in silico*

https://doi.org/10.1021/acsomega.3c01566
ACS Omega 2023, 8, 17195−17208

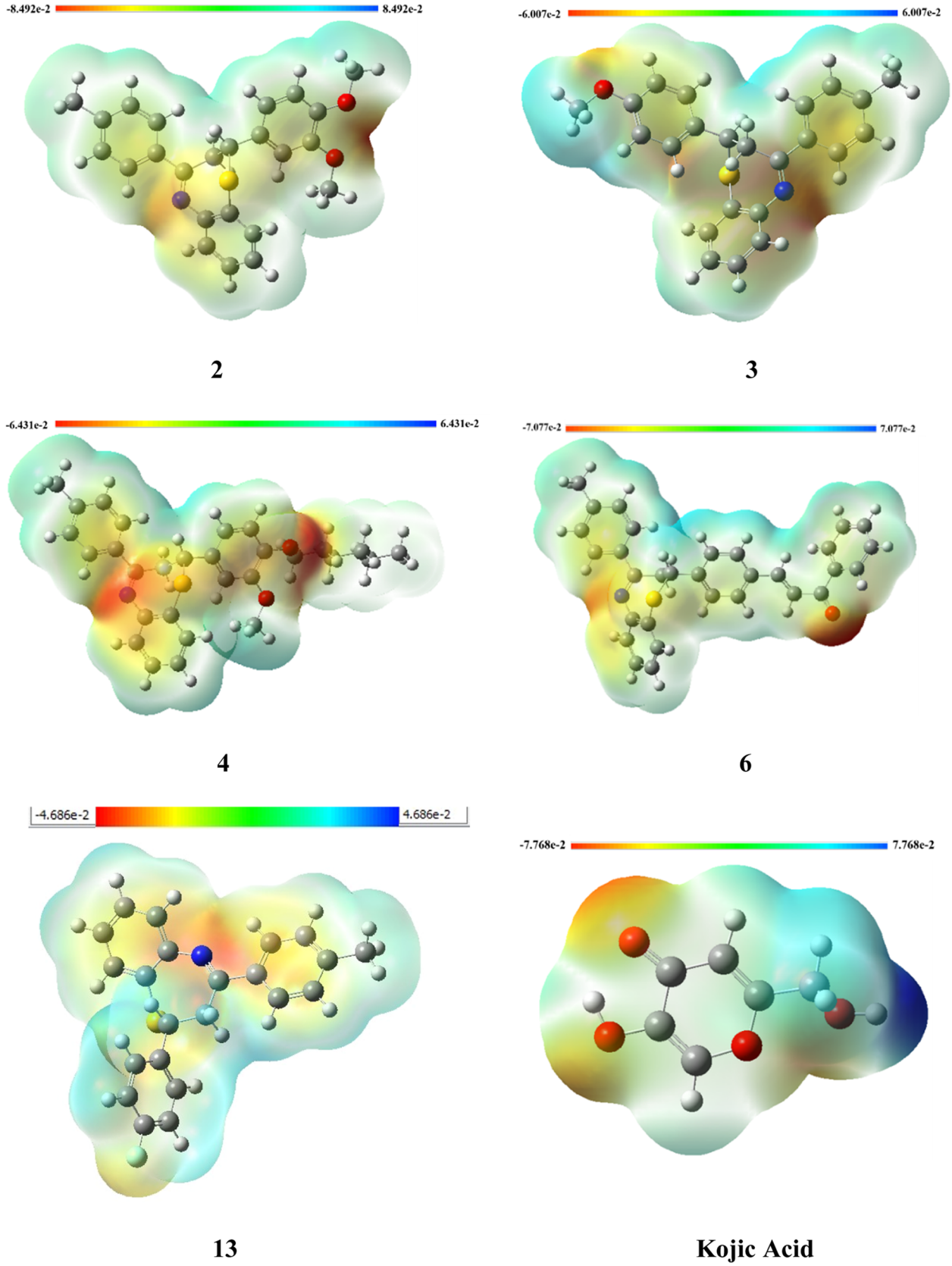

Figure 17. Molecular electrostatic potential of compounds **2**, **3**, **4**, **6**, **13**, and kojic acid.

computational examinations of all target compounds were conducted. The MD simulations ultimately demonstrated that the docked structures remained stable at the binding sites. According to druglikeness research, the majority of our compounds should not have any issues with oral bioavailability. These results give us great confidence that the compounds

https://doi.org/10.1021/acsomega.3c01566
ACS Omega 2023, 8, 17195−17208

Table 4. Calculated Molecular Properties of Benzothiazepines 1−14 for Evaluation of the Druglikeness Using Lipinski's Rule[a]

codes	molecular formula	molecular weight (g/mol)	HBA	HBD	MolLog *P* (mg/L)	MolPSA (Å^2)	mol. volume (Å^3)	druglikeness model score
1	$C_{22}H_{18}ClNS$	363.90	2	0	6.53	8.86	341.93	0.12
2	$C_{24}H_{23}NO_2S$	389.51	4	0	5.57	24.12	388.00	0.14
3	$C_{23}H_{21}NOS$	359.48	3	0	5.89	16.40	356.58	−0.04
4	$C_{29}H_{33}NO_2S$	459.64	4	0	8.07	23.99	478.69	0.27
5	$C_{26}H_{27}NO_2S$	417.56	4	0	6.61	23.99	424.97	0.46
6	$C_{31}H_{25}NOS$	459.60	3	0	7.39	21.83	469.02	−0.03
7	$C_{23}H_{19}NO_2S$	373.47	4	1	5.74	37.27	357.84	0.04
8	$C_{24}H_{23}NOS$	373.51	3	0	6.31	15.98	375.14	0.08
9	$C_{27}H_{29}NO_2S$	431.59	4	0	7.04	23.99	442.88	0.37
10	$C_{22}H_{18}N_2O_2S$	374.46	4	0	4.80	47.12	350.37	−0.29
11	$C_{22}H_{18}N_2O_2S$	374.46	4	0	4.68	47.12	350.44	−0.05
12	$C_{30}H_{27}NO_2S$	465.61	4	0	7.11	23.80	461.13	0.05
13	$C_{22}H_{18}FNS$	347.45	2	0	6.00	8.86	330.65	−0.02
14	$C_{24}H_{24}N_2S$	372.53	2	0	6.00	11.66	374.29	−0.34

[a]The table given above shows all the components of Lipinski's rule, i.e., HBA: H-bond acceptor, HBD: H-bond donor, Log *P*: lipophilicity of partition coefficient, and PSA: polar surface area.

described here could be used as a starting point for creating and developing novel TYR inhibitors.

4. EXPERIMENTAL SECTION

4.1. Mushroom TYR Inhibition Study. The mushroom TYR (Sigma Chemical) inhibition was performed in accordance with our previously published protocols.[21] 20 mL of mushroom TYR (30 U/mL), 20 mL of the inhibitor solution (inhibitor solution was prepared in dimethyl sulfoxide (DMSO), and further dilution was made by adding phosphate buffer), and 140 mL of phosphate buffer (20 mM, pH 6.8) were put into a 96-well microplate. After preincubating the test plate for 10 min at ambient temperature, 20 μL of 0.85 mM 3,4-dihydroxyphenylalanine (L-DOPA) (Sigma Chemical) was added, and the substrate L-DOPA was added at the last moment to the reaction mixture, and immediately, absorbance measurement was done.[24] Following that, the assay plate was incubated for 20 min at 25 °C. The absorbance of dopachrome at 475 nm was then measured using a microplate reader (OPTI Max, Tunable). As a reference inhibitor, kojic acid was used, while phosphate buffer served as a negative control. The percentage of concentration required to achieve 50% inhibition was used to express the amount of inhibition caused by the test substances (IC_{50}). Three separate experiments were conducted to examine each concentration. The data analysis and graphing program Origin 8.6, 64-bit calculated the IC_{50} values.

The TYR inhibition percentage was estimated as follows

$$\text{inhibition}\ (\%) = [(A - B)/A] \times 100$$

Here, *A* and *B* are the absorbances for the blank and samples, respectively.

4.1.1. Toxicity Profile of the Synthesized Derivatives. The synthesized derivatives were evaluated for their toxicity profile through *in vivo* studies.[10] The findings suggested that the target benzothiazepine derivatives are nontoxic. This fact is also supported by frequent occurrence of this pharmacophore as a structural part in various commercially available drugs.[18]

4.2. Kinetic Study of Tyrosinase Inhibitory Activity. In order to access the inhibitory kinetics, a number of experiments were carried out.[25] The Lineweaver−Burk plot of inhibitor **2** at concentrations of 0.0, 1.0, 2.0, 4.0, and 8.0 μM helps determine the kinetic mechanism. The concentration of the substrate L-DOPA varied from 0.0625 to 2 mM in each kinetic study. The preincubation and measurement periods matched those specified in the protocol for the experiment on the inhibition of mushroom TYR. After the addition of the enzyme, DOPAchrome formation was constantly observed for 5 min at intervals of 30 s in the microplate reader. The kind of inhibition on the enzyme was determined using the Lineweaver−Burk plots of inverse velocities $1/V$ *versus* inverse substrate concentration $1/[S]$ mM^{-1}.

4.3. *In Silico* Analyses. *4.3.1. Molecular Docking Assay.* To determine the potential binding orientations of the synthesized compounds **1−14** in the crystal structure of mushroom TYR, molecular docking experiments were conducted. The crystal structure of *Agaricus bisporus* TYR (PDB: 2Y9X) was obtained from the RCSB Protein Data Bank. To prepare the ligands **1−14** in their neutral form, LigPrep (Schrödinger) was used to optimize their structure in the OPLS-3 force field. The protein structure was created using one of the four monomers from the PDB entry, and the Protein Preparation (Schrödinger) program was used to add hydrogen molecules and set suitable protonation states for pH 7. The active site water molecule was placed in the center of the receptor grid box, which was specified as 20 Å × 20 Å × 20 Å. Hence, the trapped water molecule defined the receptor grid box. After docking with Glide (Schrödinger) utilizing XP precision with default values, the top 15 positions for each ligand were reported. Maestro was used to create the figures and visually evaluate the binding stances.[10,26]

4.3.2. Molecular Dynamic Simulations. To explore the stability of complex **2**, a 100 ns-long MD simulation was conducted using NAMD[27] to analyze the stability of the complex. The parameters of the ligand were generated using the Antechamber program, while the Leap program of Ambertools21[28] was used to generate the parameter topology and coordinate files. The protein residues were converted to the amber format by using the PDB4amber module. To optimize the ligand and protein structures, GAFF and ff14SB forcefields were used, respectively,[29] and TIP3P water molecules[30] were used to solvate the system in a periodic box of 10 Å. The system was further neutralized by the addition of 20 Na^+ ions. The system was then minimized to remove steric clashes for 10 000 steps, and the water equilibration was conducted for another 10 000 steps, which were then followed by further equilibrations at 200, 250, and 300 K. Finally, the system was subjected to a

https://doi.org/10.1021/acsomega.3c01566
ACS Omega 2023, 8, 17195−17208

production run for 100 ns at 310 K temperature and 1 atm pressure using the NPT ensemble. The analysis of the md trajectory was carried out using the BIO3D package of R.[31]

4.3.3. Computational (DFT) Calculations. Density functional theory (DFT) is a computational method used to calculate the energy of a molecule based on electron density instead of the wave function, resulting in more consistent findings with experimental results due to electron correlations. In this study, the 3D geometries of chromone derivatives **2**, **3**, **4**, **6**, and **13** were generated using the GaussView (5.0.16) interface and calculated in the Gaussian (v.09) program. The fundamental set 3-21G and B3LYP were used to perform DFT computations.[32] The selected compounds were optimized in DMSO solution, and frontier molecular orbital analysis was conducted. Additionally, MEP surfaces were created to determine the charge distributions within the molecules and gain insights into their interactions.

4.3.4. Druglikeness Study. The druglikeness characteristics of the target analogues **1**−**14** have been examined *in silico* using the web-based Molsoft (molsoft.com/molprop/) tool.[8]

■ ASSOCIATED CONTENT

Supporting Information

The Supporting Information is available free of charge at https://pubs.acs.org/doi/10.1021/acsomega.3c01566.

Spectral data of the reported compounds (PDF)

■ AUTHOR INFORMATION

Corresponding Authors

Zaman Ashraf − *Department of Chemistry, Allama Iqbal Open University, Islamabad 44000, Pakistan*; Email: zaman.ashraf@aiou.edu.pk

Ehsan Ullah Mughal − *Department of Chemistry, University of Gujrat, Gujrat 50700, Pakistan*; orcid.org/0000-0001-9463-9398; Email: ehsan.ullah@uog.edu.pk

Saleh A. Ahmed − *Department of Chemistry, Faculty of Applied Sciences, Umm Al-Qura University, Makkah 21955, Saudi Arabia*; orcid.org/0000-0002-2364-0380; Email: saahmed@uqu.edu.sa, saleh_63@hotmail.com

Authors

Munirah M. Al-Rooqi − *Department of Chemistry, Faculty of Applied Sciences, Umm Al-Qura University, Makkah 21955, Saudi Arabia*

Amina Sadiq − *Department of Chemistry, Govt. College Women University, Sialkot 51300, Pakistan*

Rami J. Obaid − *Department of Chemistry, Faculty of Applied Sciences, Umm Al-Qura University, Makkah 21955, Saudi Arabia*

Yasir Nazir − *Department of Chemistry, Allama Iqbal Open University, Islamabad 44000, Pakistan; Department of Chemistry, University of Sialkot, Sialkot 51300, Pakistan*

Rabab S. Jassas − *Department of Chemistry, Jamoum University College, Umm Al-Qura University, Makkah 21955, Saudi Arabia*

Nafeesa Naeem − *Department of Chemistry, University of Gujrat, Gujrat 50700, Pakistan*

Meshari A. Alsharif − *Department of Chemistry, Faculty of Applied Sciences, Umm Al-Qura University, Makkah 21955, Saudi Arabia*

Syed Wadud Ali Shah − *Department of Pharmacy, University of Malakand, Chakdara Dir 18000 Khyber Pakhtunkhwa, Pakistan*

Ziad Moussa − *Department of Chemistry, College of Science, United Arab Emirates University, 15551 Al Ain, Abu Dhabi, United Arab Emirates*; orcid.org/0000-0002-3365-0451

Abdel-Rahman Farghaly − *Department of Chemistry, College of Science, Jazan University, Jazan 114, Saudi Arabia*

Complete contact information is available at: https://pubs.acs.org/10.1021/acsomega.3c01566

Author Contributions

M.M.A.-R.: formal analysis, reviewing, and editing; A.S.: formal analysis, reviewing, and editing; R.J.O.: formal analysis, reviewing, and editing; Z.A.: enzyme inhibition and kinetic studies; Y.N.: molecular docking, simulation, and DFT studies; R.S.J.: formal analysis, reviewing, and editing; N.N.: experimental work performance, data analysis and collection, and first-draft preparation; M.A.A.: formal analysis, reviewing, and editing; S.W.A.S.: formal analysis, reviewing, and editing; Z.M.: formal analysis, reviewing, and editing; E.U.M.: main idea, supervision, final writing of the article, and funding acquisition; A.-R.F.: formal analysis, reviewing, and editing; S.A.A.: main idea, supervision, final writing of the article, and funding acquisition.

Notes

The authors declare no competing financial interest.

■ ACKNOWLEDGMENTS

The authors would like to thank the Deanship of Scientific Research at Umm Al-Qura University for supporting this work by Grant code: (23UQU4320545DSR001). The financial support by the Higher Education Commission of Pakistan (HEC) under Project No. (NRPU-15800) is gratefully acknowledged. Dr. Z.M. is grateful to United Arab Emirates University (UAEU) and to the Research Office for supporting the research developed in his laboratory and reported herein (SUREPLUS Grant code G00003918).

■ REFERENCES

(1) (a) Pillaiyar, T.; Manickam, M.; Namasivayam, V. Skin whitening agents: Medicinal chemistry perspective of tyrosinase inhibitors. *J. Enzyme Inhib. Med. Chem.* **2017**, *32*, 403−425. (b) Lee, S. Y.; Baek, N.; Nam, T.-g. Natural, semisynthetic and synthetic tyrosinase inhibitors. *J. Enzyme Inhib. Med. Chem.* **2016**, *31*, 1−13.

(2) (a) Chung, K. W.; Park, Y. J.; Choi, Y. J.; Park, M. H.; Ha, Y. M.; Uehara, Y.; Yoon, J. H.; Chun, P.; Moon, H. R.; Chung, H. Y. Evaluation of in vitro and in vivo anti-melanogenic activity of a newly synthesized strong tyrosinase inhibitor (E)-3-(2, 4 dihydroxybenzylidene) pyrrolidine-2, 5-dione (3-DBP). *Biochim. Biophys. Acta, Gen. Subj.* **2012**, *1820*, 962−969. (b) Kang, S. S.; Kim, H. J.; Jin, C.; Lee, Y. S. Synthesis of tyrosinase inhibitory (4-oxo-4H-pyran-2-yl) acrylic acid ester derivatives. *Bioorg. Med. Chem. Lett.* **2009**, *19*, 188−191.

(3) (a) Xie, J.; Dong, H.; Yu, Y.; Cao, S. Inhibitory effect of synthetic aromatic heterocycle thiosemicarbazone derivatives on mushroom tyrosinase: Insights from fluorescence, 1H NMR titration and molecular docking studies. *Food Chem.* **2016**, *190*, 709−716. (b) Hałdys, K.; Latajka, R. Thiosemicarbazones with tyrosinase inhibitory activity. *MedChemComm* **2019**, *10*, 378−389.

(4) (a) Butt, A. R. S.; Abbasi, M. A.; Siddiqui, S. Z.; Raza, H.; Hassan, M.; Shah, S. A. A.; Seo, S.-Y. Synthesis, Kinetics, Binding Conformations and Structure-activity Relationship of Potent Tyrosinase Inhibitors: Aralkylated 2-aminothiazole-ethyltriazole Hybrids. *Iran. J. Pharm. Res.* **2021**, *20*, 206. (b) Li, J.; Feng, L.; Liu, L.; Wang, F.;

Ouyang, L.; Zhang, L.; Hu, X.; Wang, G. Recent advances in the design and discovery of synthetic tyrosinase inhibitors. *Eur. J. Med. Chem.* **2021**, *224*, No. 113744.
(5) Al-Warhi, T.; Elimam, D. M.; Elsayed, Z. M.; Abdel-Aziz, M. M.; Maklad, R. M.; Al-Karmalawy, A. A.; Afarinkia, K.; Abourehab, M. A.; Abdel-Aziz, H. A.; Eldehna, W. M. Development of novel isatin thiazolyl-pyrazoline hybrids as promising antimicrobials in MDR pathogens. *RSC Adv.* **2022**, *12*, 31466−31477.
(6) (a) Peng, Z.; Wang, G.; Zeng, Q.-H.; Li, Y.; Liu, H.; Wang, J. J.; Zhao, Y. A systematic review of synthetic tyrosinase inhibitors and their structure-activity relationship. *Crit. Rev. Food Sci. Nutr.* **2022**, *62*, 4053−4094. (b) Samir, M.; Ramadan, M.; Abdelrahman, M. H.; Abdelbaset, M. S.; Abourehab, M. A.; Abdel-Aziz, M.; Abuo-Rahma, G. E.-D. A. 3, 7-bis-benzylidene hydrazide ciprofloxacin derivatives as promising antiproliferative dual TOP I & TOP II isomerases inhibitors. *Bioorg. Chem.* **2021**, *110*, No. 104698. (c) Aljuhani, E.; Aljohani, M. M.; Alsoliemy, A.; Shah, R.; Abumelha, H. M.; Saad, F. A.; Hossan, A.; Al-Ahmed, Z. A.; Alharbi, A.; El-Metwaly, N. M. Synthesis and characterization of Cu (II)-pyrazole complexes for possible anticancer agents; conformational studies as well as compatible in-silico and in-vitro assays. *Heliyon* **2021**, *7*, No. e08485.
(7) (a) Zolghadri, S.; Bahrami, A.; Hassan Khan, M. T.; Munoz-Munoz, J.; Garcia-Molina, F.; Garcia-Canovas, F.; Saboury, A. A. A comprehensive review on tyrosinase inhibitors. *J. Enzyme Inhib. Med. Chem.* **2019**, *34*, 279−309. (b) Sudha, D.; Kumar, E. R.; Shanjitha, S.; Munshi, A. M.; Al-Hazmi, G. A.; El-Metwaly, N. M.; Kirubavathy, S. J. Structural, optical, morphological and electrochemical properties of ZnO and graphene oxide blended ZnO nanocomposites. *Ceram. Int.* **2023**, *49*, 7284−7288. (c) Azher, O. A.; Hossan, A.; Pashameah, R. A.; Alsoliemy, A.; Alharbi, A.; Habeebullah, T. M.; El-Metwaly, N. M. Synthesis, anticancer evaluation, and molecular modeling study of new 2-(phenylamino) pyrazolo [1, 5-a] pyrimidine analogues. *Arab. J. Chem.* **2023**, *16*, No. 104437. (d) Alkhatib, F. M.; Farghaly, T. A.; Harras, M. F.; El-Ghamry, H. A. Copper (II) complexes based on 1, 3, 4-thiadiazolethiosemicarbazone NNS donor ligands: synthesis, molecular structure, DNA binding and in silico molecular docking approach. *Inorg. Nano-Metal Chem.* **2021**, 1−12.
(8) Alsantali, R. I.; Mughal, E. U.; Naeem, N.; Alsharif, M. A.; Sadiq, A.; Ali, A.; Jassas, R. S.; Javed, Q.; Javid, A.; Sumrra, S. H.; et al. Flavone-based hydrazones as new tyrosinase inhibitors: Synthetic imines with emerging biological potential, SAR, molecular docking and drug-likeness studies. *J. Mol. Struct.* **2022**, *1251*, No. 131933.
(9) (a) Gardelly, M.; Trimech, B.; Belkacem, M. A.; Harbach, M.; Abdelwahed, S.; Mosbah, A.; Bouajila, J.; Jannet, H. B. Synthesis of novel diazaphosphinanes coumarin derivatives with promoted cytotoxic and anti-tyrosinase activities. *Bioorg. Med. Chem. Lett.* **2016**, *26*, 2450−2454. (b) Huang, Y.; Yang, J.; Chi, Y.; Gong, C.; Yang, H.; Zeng, F.; Gao, F.; Hua, X.; Wang, Z. Newly Designed Quinazolinone Derivatives as Novel Tyrosinase Inhibitor: Synthesis, Inhibitory Activity, and Mechanism. *Molecules* **2022**, *27*, No. 5558. (c) Vanjare, B. D.; Choi, N. G.; Mahajan, P. G.; Raza, H.; Hassan, M.; Han, Y.; Yu, S.-M.; Kim, S. J.; Seo, S.-Y.; Lee, K. H. Novel 1, 3, 4-oxadiazole compounds inhibit the tyrosinase and melanin level: Synthesis, in-vitro, and in-silico studies. *Bioorg. Med. Chem.* **2021**, *41*, No. 116222.
(10) Mehmood, R.; Mughal, E. U.; Elkaeed, E. B.; Obaid, R. J.; Nazir, Y.; Al-Ghulikah, H. A.; Naeem, N.; Al-Rooqi, M. M.; Ahmed, S. A.; Shah, S. W. A.; Sadiq, A. Synthesis of novel 2, 3-dihydro-1, 5-benzothiazepines as α-glucosidase inhibitors: In vitro, in vivo, kinetic, SAR, molecular docking, and QSAR studies. *ACS Omega* **2022**, *7*, 30215−30232.
(11) Hu, Y.-G.; Gao, Z.-P.; Zheng, Y.-Y.; Hu, C.-M.; Lin, J.; Wu, X.-Z.; Zhang, X.; Zhou, Y.-S.; Xiong, Z.; Zhu, D.-Y. Synthesis and Biological Activity Evaluation of 2-Cyanopyrrole Derivatives as Potential Tyrosinase Inhibitors. *Front. Chem.* **2022**, No. 914944.
(12) Zolghadri, S.; Bahrami, A.; Hassan Khan, M. T.; Munoz-Munoz, J.; Garcia-Molina, F.; Garcia-Canoras, F.; Sabour, A. A. A comprehensive review on tyrosinase inhibitors. *J. Enzyme Inhib. Med. Chem.* **2019**, *34*, 279−309.
(13) (a) Masum, M. N.; Yamauchi, K.; Mitsunaga, T. Tyrosinase inhibitors from natural and synthetic sources as skin-lightening agents. *Rev. Agric. Sci.* **2019**, *7*, 41−58. (b) Roulier, B.; Pérès, B.; Haudecoeur, R. Advances in the design of genuine human tyrosinase inhibitors for targeting melanogenesis and related pigmentations. *J. Med. Chem.* **2020**, *63*, 13428−13443. (c) Obaid, R. J.; Mughal, E. U.; Naeem, N.; Sadiq, A.; Alsantali, R. I.; Jassas, R. S.; Moussa, Z.; Ahmed, S. A. Natural and synthetic flavonoid derivatives as new potential tyrosinase inhibitors: A systematic review. *RSC Adv.* **2021**, *11*, 22159−22198.
(14) Mehmood, R.; Mughal, E. U.; Elkaeed, E. B.; Obaid, R. J.; Nazir, Y.; Al-Ghulikah, H. A.; Naeem, N.; Al-Rooqi, M. M.; Ahmed, S. A.; Shah, S. W. A.; Sadiq, A. Synthesis of Novel 2, 3-Dihydro-1, 5-Benzothiazepines as α-Glucosidase Inhibitors: In Vitro, In Vivo, Kinetic, SAR, Molecular Docking, and QSAR Studies. *ACS Omega* **2022**, *7*, 30215.
(15) Li, T.; Zhang, J.; Pan, J.; Wu, Z.; Hu, D.; Song, B. Design, synthesis, and antiviral activities of 1, 5-benzothiazepine derivatives containing pyridine moiety. *Eur. J. Med. Chem.* **2017**, *125*, 657−662.
(16) (a) Bariwal, J. B.; Upadhyay, K. D.; Manvar, A. T.; Trivedi, J. C.; Singh, J. S.; Jain, K. S.; Shah, A. K. 1, 5-Benzothiazepine, a versatile pharmacophore: a review. *Eur. J. Med. Chem.* **2008**, *43*, 2279−2290. (b) Ul-Haq, Z.; Khan, W.; Kalsoom, S.; Ansari, F. L. In silico modeling of the specific inhibitory potential of thiophene-2,3-dihydro-1,5-benzothiazepine against BChE in the formation of β-amyloid plaques associated with Alzheimer's disease. *Theor. Biol. Med. Modell.* **2010**, *7*, 1−26. (c) Albanese, D. C. M.; Gaggero, N.; Fei, M. A practical synthesis of 2, 3-dihydro-1, 5-benzothiazepines. *Green Chem.* **2017**, *19*, 5703−5707. (d) Saha, D.; Jain, G.; Sharma, A. Benzothiazepines: Chemistry of a privileged scaffold. *RSC Adv.* **2015**, *5*, 70619−70639.
(17) (a) Feng, M.; Tang, B.; H Liang, S.; Jiang, X. Sulfur containing scaffolds in drugs: synthesis and application in medicinal chemistry. *Curr. Top. Med. Chem.* **2016**, *16*, 1200−1216. (b) Pathania, S.; Narang, R. K.; Rawal, R. K. Role of sulphur-heterocycles in medicinal chemistry: An update. *Eur. J. Med. Chem.* **2019**, *180*, 486−508. (c) Arora, P.; Arora, V.; Lamba, H.; Wadhwa, D. Importance of heterocyclic chemistry: a review. *Int. J. Pharm. Sci. Res.* **2012**, *3*, 2947.
(18) Chen, S.-Q.; Ding, F.; Liu, F.-M. Investigation on the Ring-Opening Reactions of 3-(1H-1, 2, 4-Triazol-1-yl) 1, 5-benzothiazepines with Arylonitrile Oxides. *Phosphorus, Sulfur Silicon Relat. Elem.* **2011**, *186*, 574−581.
(19) Haroun, M.; Chobe, S. S.; Alavala, R. R.; Mathure, S. M.; Jamullamudi, R. N.; Nerkar, C. K.; Gugulothu, V. K.; Tratrat, C.; Islam, M. M.; Venugopala, K. N.; et al. 1,5-Benzothiazepine Derivatives: Green Synthesis, In Silico and In Vitro Evaluation as Anticancer Agents. *Molecules* **2022**, *27*, No. 3757.
(20) Ashraf, J.; Mughal, E. U.; Sadiq, A.; Bibi, M.; Naeem, N.; Ali, A.; Massadaq, A.; Fatima, N.; Javid, A.; Zafar, M. N.; et al. Exploring 3-hydroxyflavone scaffolds as mushroom tyrosinase inhibitors: synthesis, X-ray crystallography, antimicrobial, fluorescence behaviour, structure-activity relationship and molecular modelling studies. *J. Biomol. Struct. Dyn.* **2021**, *39*, 7107−7122.
(21) Nazir, Y.; Rafique, H.; Kausar, N.; Abbas, Q.; Ashraf, Z.; Rachtanapun, P.; Jantanasakulwong, K.; Ruksiriwanich, W. Methoxy-substituted tyramine derivatives synthesis, computational studies and tyrosinase inhibitory kinetics. *Molecules* **2021**, *26*, No. 2477.
(22) (a) Nazir, Y.; Saeed, A.; Rafiq, M.; Afzal, S.; Ali, A.; Latif, M.; Zuegg, J.; Hussein, W. M.; Fercher, C.; Barnard, R. T.; et al. Hydroxyl substituted benzoic acid/cinnamic acid derivatives: Tyrosinase inhibitory kinetics, anti-melanogenic activity and molecular docking studies. *Bioorg. Med. Chem. Lett.* **2020**, *30*, No. 126722. (b) Nazir, Y.; Rafique, H.; Roshan, S.; Shamas, S.; Ashraf, Z.; Rafiq, M.; Tahir, T.; Qureshi, Z.-U.-R.; Aslam, A.; Asad, M. H. H. B. Molecular Docking, synthesis, and tyrosinase inhibition activity of acetophenone amide: Potential inhibitor of melanogenesis. *BioMed Res. Int.* **2022**, No. 1040693. (c) Rafiq, M.; Nazir, Y.; Ashraf, Z.; Rafique, H.; Afzal, S.; Mumtaz, A.; Hassan, M.; Ali, A.; Afzal, K.; Yousuf, M. R.; et al. Synthesis, computational studies, tyrosinase inhibitory kinetics and antimelanogenic activity of hydroxy substituted 2-[(4-acetylphenyl)

https://doi.org/10.1021/acsomega.3c01566
ACS Omega 2023, 8, 17195−17208

amino]-2-oxoethyl derivatives. *J. Enzyme Inhib. Med. Chem.* **2019**, *34*, 1562−1572.
(23) Khurshid, A.; Saeed, A.; Erben, M. F.; Hökelek, T.; Jabeen, E. DFT guided substitution effect on azomethine reactive center in newly synthesized Schiff base aromatic scaffolds; syntheses, characterization, single crystal XRD, Hirshfeld surface and crystal void analyses. *J. Mol. Struct.* **2023**, *1273*, No. 134215.
(24) (a) Qin, H.-L.; Shang, Z.-P.; Jantan, I.; Tan, O. U.; Hussain, M. A.; Sher, M.; Bukhari, S. N. A. Molecular docking studies and biological evaluation of chalcone based pyrazolines as tyrosinase inhibitors and potential anticancer agents. *RSC Adv.* **2015**, *5*, 46330−46338. (b) Tang, J.; Liu, J.; Wu, F. Molecular docking studies and biological evaluation of 1, 3, 4-thiadiazole derivatives bearing Schiff base moieties as tyrosinase inhibitors. *Bioorg. Chem.* **2016**, *69*, 29−36. (c) Zhu, T.-H.; Cao, S.-W.; Yu, Y.-Y. Synthesis, characterization and biological evaluation of paeonol thiosemicarbazone analogues as mushroom tyrosinase inhibitors. *Int. J. Biol. Macromol.* **2013**, *62*, 589−595. (d) Varela, M. T.; Ferrarini, M.; Mercaldi, V. G.; da Silva Sufi, B.; Padovani, G.; Nazato, L. I. S.; Fernandes, J. P. S. Coumaric acid derivatives as tyrosinase inhibitors: Efficacy studies through in silico, in vitro and ex vivo approaches. *Bioorg. Chem.* **2020**, *103*, No. 104108.
(25) Ashraf, Z.; Rafiq, M.; Seo, S.-Y.; Kwon, K. S.; Babar, M. M.; Sadaf Zaidi, N.-u.-S. Kinetic and in silico studies of novel hydroxy-based thymol analogues as inhibitors of mushroom tyrosinase. *Eur. J. Med. Chem.* **2015**, *98*, 203−211.
(26) Mary, Y. S.; Mary, Y. S.; Armaković, S.; Armaković, S. J.; Krátký, M.; Vinsova, J.; Baraldi, C.; Gamberini, M. C. Concentration and solvent dependent SERS, DFT, MD simulations and molecular docking studies of a thioxothiazolidine derivative with antimicrobial properties. *J. Mol. Liq.* **2021**, *329*, No. 115582.
(27) Phillips, J. C.; Hardy, D. J.; Maia, J. D.; Stone, J. E.; Ribeiro, J. V.; Bernardi, R. C.; Buch, R.; Fiorin, G.; Hénin, J.; Jiang, W.; et al. Scalable molecular dynamics on CPU and GPU architectures with NAMD. *J. Chem. Phys.* **2020**, *153*, No. 044130.
(28) Case, D. A.; Aktulga, H. M.; Belfon, K.; Ben-Shalom, I.; Brozell, S. R.; Cerutti, D.; Cheatham, T.; Cruzeiro, V. W. D.; Darden, T.; Duke, R. E.et al. *Amber 2021: Reference Manual*; University of California: San Francisco, 2021.
(29) Duan, Y.; Wu, C.; Chowdhury, S.; Lee, M. C.; Xiong, G.; Zhang, W.; Yang, R.; Cieplak, P.; Luo, R.; Lee, T.; et al. A point-charge force field for molecular mechanics simulations of proteins based on condensed-phase quantum mechanical calculations. *J. Comput. Chem.* **2003**, *24*, 1999−2012.
(30) Jorgensen, W. L.; Chandrasekhar, J.; Madura, J. D.; Impey, R.W.; Klein, M. L. Comparison of Simple Potential Functions for Simulating Liquid Water. *J. Chem. Phys.* **1983**, *79*, 926.
(31) Grant, B. J.; Skjærven, L.; Yao, X. Q. The Bio3D packages for structural bioinformatics. *Protein Sci.* **2021**, *30*, 20−30.
(32) (a) Ashraf, J.; Mughal, E. U.; Alsantali, R. I.; Sadiq, A.; Jassas, R. S.; Naeem, N.; Ashraf, Z.; Nazir, Y.; Zafar, M. N.; Mumtaz, A.; et al. 2-Benzylidenebenzofuran-3 (2 H)-ones as a new class of alkaline phosphatase inhibitors: synthesis, SAR analysis, enzyme inhibitory kinetics and computational studies. *RSC Adv.* **2021**, *11*, 35077−35092. (b) Frisch, M.; Trucks, G.; Schlegel, H.; Scuseria, G.; Robb, M.; Cheeseman, J.; Scalmani, G.; Barone, V.; Mennucci, B.; Petersson, G. *Gaussian 09*, revision D.01; Gaussian, Inc.: Wallingford, CT, 2009. http://www.gaussian.com. See also: URL (c) Hayani, S.; Sert, Y.; Baba, Y. F.; Benhiba, F.; Chahdi, F. O.; Laraqui, F.-Z.; Mague, J. T.; El Ibrahimi, B.; Sebbar, N. K.; Rodi, Y. K.; Essassi, E. M. New alkyl (cyclohexyl) 2-oxo-1-(prop-2-yn-1-yl)-1, 2-dihydroquinoline-4-carboxylates: Synthesis, crystal structure, spectroscopic characterization, hirshfeld surface analysis, molecular docking studies and DFT calculations. *J. Mol. Struct.* **2021**, *1227*, No. 129520. (d) Mendoza-Huizar, L. H.; Rios-Reyes, C. H.; Zuñiga-Trejo, H. A computational study of the chemical reactivity of isoxaflutole herbicide and its active metabolite using global and local descriptors. *J. Serb. Chem. Soc.* **2020**, *85*, 1163−1174.

https://doi.org/10.1021/acsomega.3c01566
ACS Omega 2023, 8, 17195−17208